Supporting Information

In situ sulfuration synthesis of heterostructure MoS_2-Mo_2C@C for boosting photocatalytic H_2-production activity of TiO_2

Jinfeng Liu[a], Ping Wang[*a], Lulu Gao[a], Xuefei Wang[a], Huogen Yu[*ab]

[a] School of Chemistry, Chemical Engineering and Life Sciences and School of Materials Science and Engineering, Wuhan University of Technology, Wuhan, 430070, P. R. China

[b] Laboratory of Solar Fuel, Faculty of Materials Science and Chemistry, China University of Geosciences, Wuhan, 430074, P. R. China

*Corresponding authors. Tel: +86(27)87749379;

E-mail: wangping0904@whut.edu.cn (Ping Wang);

huogenyu@163.com (Huogen Yu)

SI Experimental

SI-1 Materials

Titanium dioxide (TiO_2-P25), sulfur powder (S), ammonium heptamolybdate ($(NH_4)_6Mo_7O_{24}\cdot 4H_2O$, AR), cadmium nitrate ($Cd(NO_3)_2\cdot 4H_2O$), Zinc nitrate ($Zn(NO_3)_2\cdot 6H_2O$), sodium sulfide ($Na_2S\cdot 9H_2O$), sodium sulfate ($Na_2SO_4$), methanol ($CH_3OH$), and ethyl alcohol ($C_2H_5OH$) were of analytical grade from Shanghai Chemical Reagent Ltd. (PR China) and used without further purification.

SI-2 Based on the XRD patterns, the weight ratio of MoS_2 and Mo_2C in the MoS_2-Mo_2C@C samples can be estimated using the following formula S1 [Ref. S1]:

$$W_A = \frac{I_A}{I_A + (I_B/(RIR_B/RIR_A))}$$

$$W_B = \frac{I_B}{I_B + (I_A/(RIR_A/RIR_B))} \qquad S1$$

where I_A and I_B are the intensities of the strongest lines of the X-ray diffraction patterns of MoS_2 and Mo_2C, respectively. The *RIR* values of MoS_2 (JCPDS Card No. 37-1492) and Mo_2C (JCPDS Card No. 35-0787) were obtained by the matrix-flushing method according to the Chung's report [Ref. S2].

SI-3 Characterization

X-ray diffraction (XRD) (D/MAXRB, RIGAKU, Japan), FTIR (Nicolet 6700, Thermo Electron Scientific Instruments, USA)，Raman microscope (InVia, Renishaw, UK), and transmission electron microscopy (TEM) (Talos F200S, Thermo Fisher, USA) with an energy-dispersive X-ray spectroscopy (EDS) were used to

character the microstructures and morphologies of the photocatalysts. Nitrogen adsorption-desorption isotherms were analyzed by a nitrogen adsorption-desorption apparatus (ASAP 2020, Micromeritics, USA). Elemental analyses were characterized X-ray photoelectron spectroscopy (XPS) (ESCALAB 250Xi, Thermo Scientific, USA). UV-vis spectrophotometer (UV-2450, Shimadzu, Japan) was used to perform the optical absorption property. Time-resolved photoluminescence (TRPL) (FLS920, Edinburgh Instruments, UK) was applied to measure the fluorescence lifetimes.

SI-4 Photoelectrochemical measurements

Photoelectrochemical curves were measured on an electrochemical analyzer (CHI660E, China) in a standard three-electrode configuration. The prepared samples were loaded on fluorine-doped tin oxide (FTO) conductor glass, a standard Ag/AgCl electrode and a platinum foil as the working electrodes, reference electrode and counter electrode, respectively, with Na_2SO_4 (0.5 M) as electrolyte solution. The working electrodes were prepared on fluorine-doped tin oxide (FTO) conductor glass in a typically method. First, photocatalysts (4 mg) were dispersed in a solution which mixed with 1 mL of anhydrous ethanol and 100 μL of D-520 Nafion solution (5%, w/w, in water and 1-propanol, Alfa Aesar), and then ultrasonicated for 30 min to achieve the suspension solution. The suspension was spread on the FTO glass which dried at 60^{o}C for one night. Linear sweep voltammetry (LSV) curves were obtained in the potential ranging of -0.4 to -1.5 V with a scan rate of 10 mV s^{-1}. Transient photocurrent responses (*i-t*) curves were conducted at a static potential of +0.5 V.

Electrochemical impedance spectroscopy (EIS) was performed at a frequency range of 10^{-2}-10^{4} Hz. The Mott-Schottky plots were measured at a fixed frequency of 3000 Hz to determine the flat band potential. A 3W LED lamp (365 nm) was served as the irradiator.

SI-5 Measurement of photocatalytic hydrogen evolution

Photocatalytic hydrogen production activity was evaluated with 50 mg of photocatalyst dispersed in a 100 mL three-necked Pyrex glass containing 80 mL of methyl alcohol (10 vol%) under four LEDs (3 W, 365 nm, Shenzhen Lamplic Science Co. Ltd., China). The system was bubbled with N_2 for 15 min to guarantee hydrogen production process occurring in an inert atmosphere. After four 365 nm-LED lights irradiated the system, 400 μL of gas was injected into a gas chromatograph (Shimadzu, GC-2014C, Japan) with a thermal conductivity detector and a 5 Å molecular sieve column with nitrogen as a carrier gas. The apparent quantum efficiency (AQE) was calculated according to the equation S2:

$$AQE(\%) = \frac{number\ of\ reacted\ electrons}{number\ of\ incident\ photons} \times 100\%$$

$$= \frac{number\ of\ evolved\ H_2\ molecules \times 2}{number\ of\ incident\ photons} \times 100\% \quad S2$$

SI-6 Fluorescent lifetime of the samples

The lifetime of photogenerated charge carries of samples are fitted by a biexponential function as the equation S3 [Ref 3]:

$$I(t) = A_1\exp(-t/\tau_1) + A_2\exp(-t/\tau_2) \quad S3$$

where τ_1 and τ_2 are the lifetime of photogenerated charge carries, and A_1, and A_2 are

the corresponding amplitudes. The short lifetime component for τ_1 represents the radiation-recombination time of photogenerated carriers, while the longer lifetime component for τ_2 originates from the nonradioactive recombination of the relaxation effect for photogenerated charges and the τ_{av} represents the average excited-state lifetime.

References

[1] Y. Lu, J. Zhang, F. Wang, X. Chen, Z. Feng, and C. Li, K_2SO_4-assisted hexagonal/monoclinic WO_3 phase junction for efficient photocatalytic degradation of RhB. ACS Applied Energy Materials, 1 (2018) 2067-2077.

[2] H. Frank, Quantitative interpretation of X-ray diffraction patterns of mixtures. I. matrix-flushing method for quantitative multicomponent analysis. Journal of Applied Crystal 7 (1974) 519-525.

[3] X. Wang, C. Liow, A. Bisht, X. Liu, T. Sum, X. Chen, S. Li, Engineering interfacial photo-induced charge transfer based on nanobamboo array architecture for efficient solar-to-chemical energy conversion, Advanced Materials, 27 (2015) 2207-2214.

Figure captions

Fig. S1 Nitrogen adsorption-desorption isotherms of (a) TiO_2, (b) Mo_2C@C/TiO_2, (c) MoS_2-Mo_2C@C/TiO_2, and (d) MoS_2@C/TiO_2.

Fig. S2 The photocatalytic H_2-evolution performance of MoS_2-Mo_2C@C/TiO_2 photocatalyst under different pH value (A) and methanol concentration (B).

Fig. S3 (A) XRD patterns and (B) XPS spectra of Mo 3d for the MoS_2-Mo_2C@C/TiO_2 sample: (a) before and (b) after the cyclic photocatalytic hydrogen-production reaction.

Fig. S4 Linear sweep voltammetry curves of (a) Mo_2C@C, (b) MoS_2-Mo_2C@C, and (c) MoS_2@C.

Fig. S5 Mott-Schottky plots of (a) TiO_2 and (b) MoS_2-Mo_2C@/TiO_2 photocatalyst in

Fig. S5 Mott-Schottky plots of (a) TiO_2 and (b) MoS_2-Mo_2C@/TiO_2 photocatalyst in

Na_2SO_4 solution (0.1 mol L^{-1}).

Fig. S6 (A, B) XRD patterns and (C, D) UV-vis spectra of (a) CdS, (a') MoS_2-Mo_2C@C/CdS, (b) ZnS, and (b') MoS_2-Mo_2C@C/ZnS.

Table S1 The specific surface area and pore volume of various photocatalysts.

Samples	Specific surface area ($m^2\ g^{-1}$)	Pore volume ($cm^3\ g^{-1}$)
TiO_2	54.41	0.52
Mo_2C@C/TiO_2	45.58	0.60
MoS_2-Mo_2C@C/TiO_2	44.05	0.63
MoS_2@C/TiO_2	42.11	0.57

Table S2 The H_2-evolution performance and apparent quantum efficiency (AQE) of the various samples.

Samples	H_2-evolution rate ($\mu mol\ h^{-1}\ g^{-1}$)	AQE (%)
TiO_2	10	0.03
MoS_2-Mo_2C@C-500/TiO_2	860	2.58
MoS_2-Mo_2C@C-600/TiO_2	940	2.82
MoS_2-Mo_2C@C-700/TiO_2 (MoS_2-Mo_2C@C/TiO_2)	1160	3.48
MoS_2-Mo_2C@C-800/TiO_2	800	2.4
Mo_2C@C/TiO_2	610	1.83
MoS_2@C/TiO_2	300	0.9

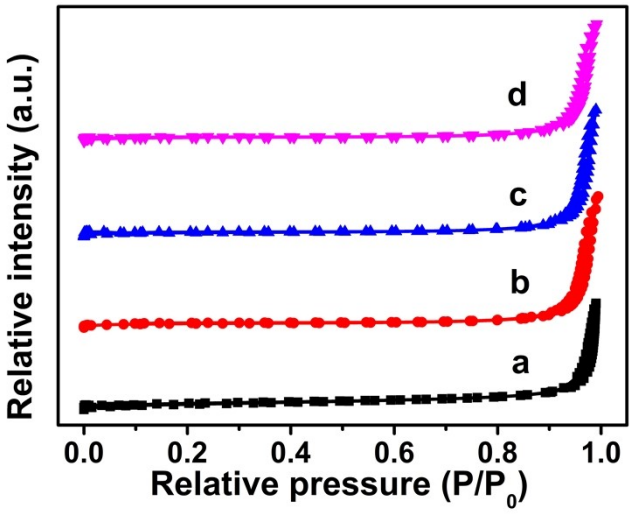

Fig. S1 Nitrogen adsorption-desorption isotherms of (a) TiO_2, (b) Mo_2C@C/TiO_2, (c) MoS_2-Mo_2C@C/TiO_2, and (d) MoS_2@C/TiO_2.

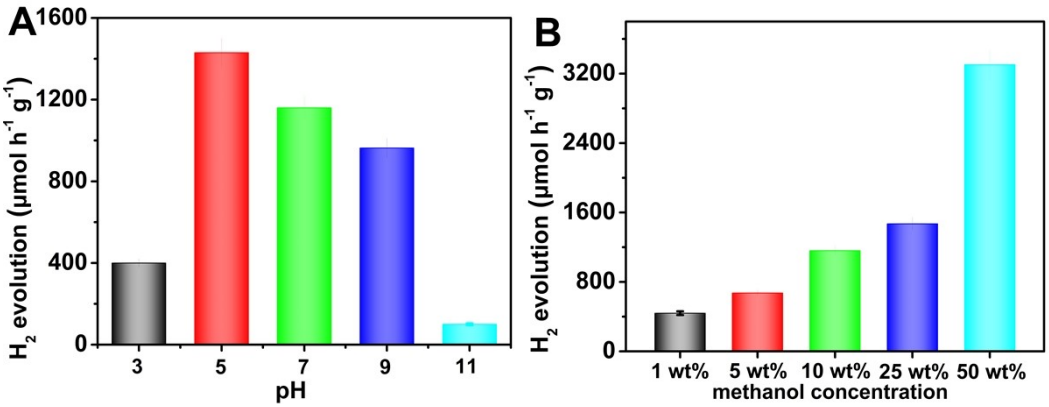

Fig. S2 The photocatalytic H_2-evolution performance of MoS_2-Mo_2C@C/TiO_2 photocatalyst under different pH value (A) and methanol concentration (B).

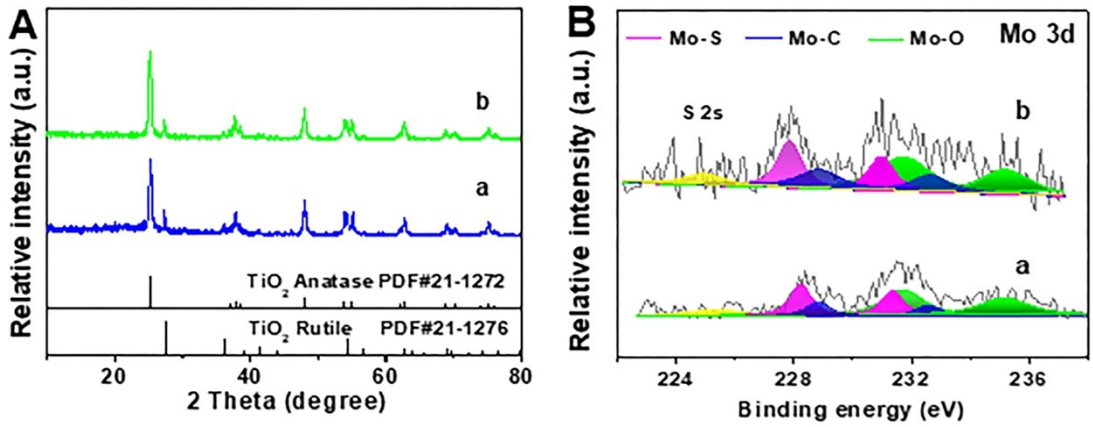

Fig. S3 (A) XRD patterns and (B) XPS spectra of Mo 3d for the MoS_2-Mo_2C@C/TiO_2 sample: (a) before and (b) after the cyclic photocatalytic hydrogen-production reaction.

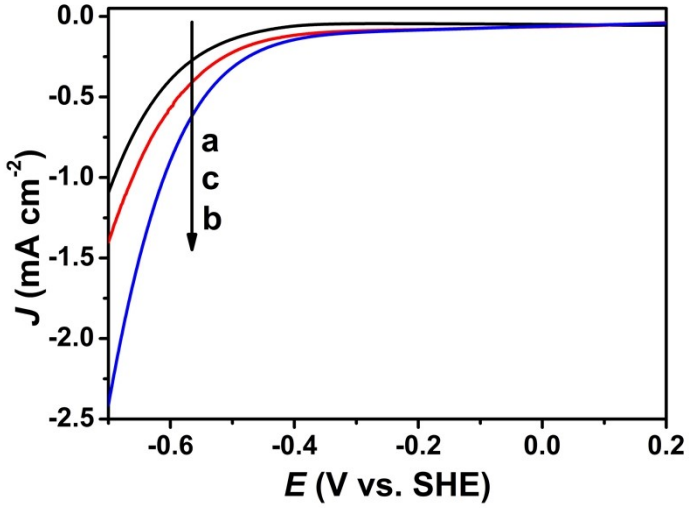

Fig. S4 Linear sweep voltammetry curves of (a) Mo_2C@C, (b) MoS_2-Mo_2C@C, and (c) MoS_2@C.

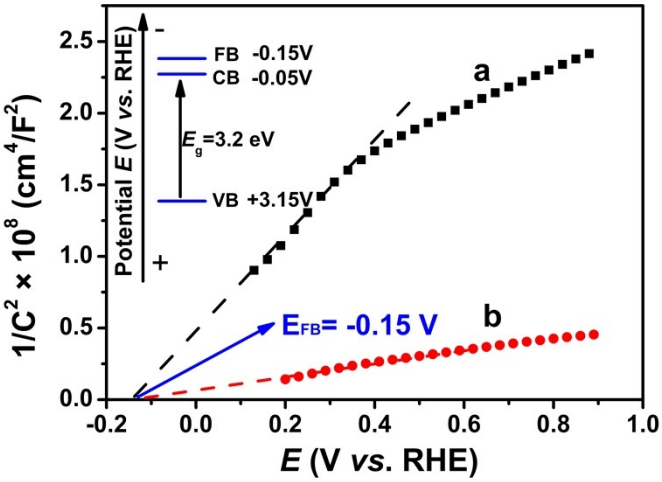

Fig. S5 Mott-Schottky plots of (a) TiO_2 and (b) MoS_2-Mo_2C@/TiO_2 photocatalyst in Na_2SO_4 solution (0.1 mol L^{-1}).

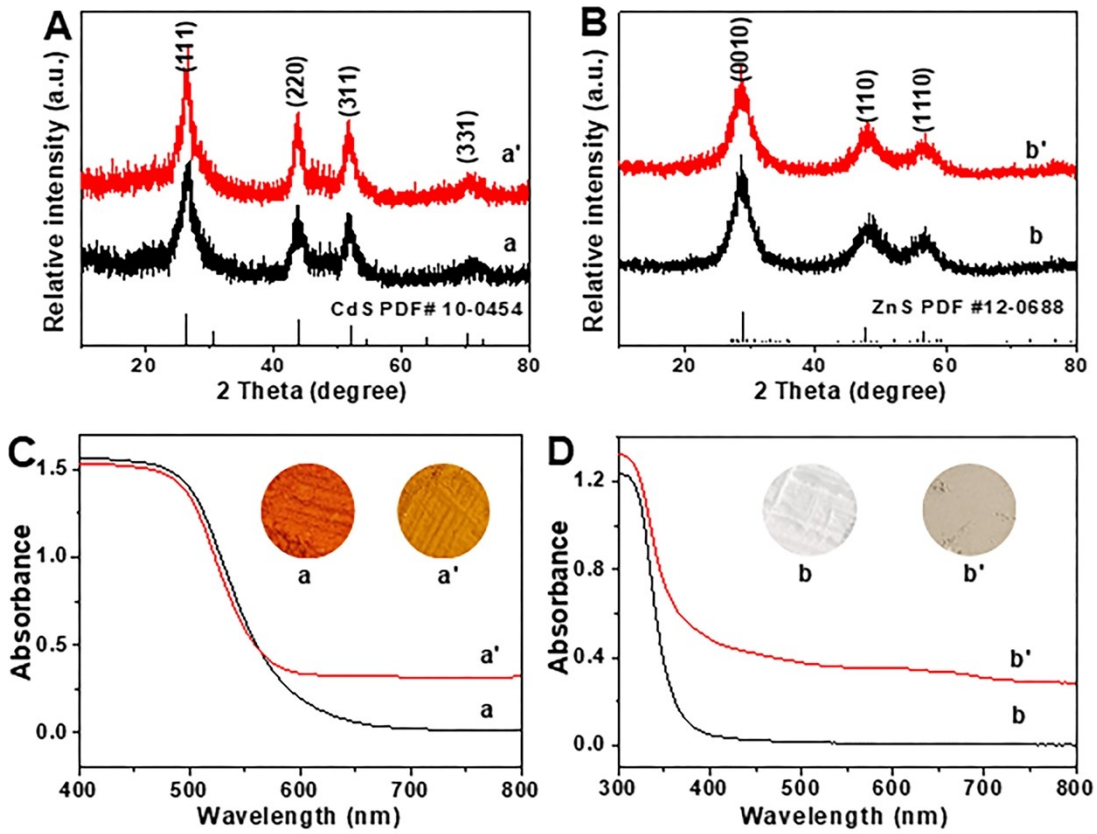

Fig. S6 (A, B) XRD patterns and (C, D) UV-vis spectra of (a) CdS, (a') MoS_2-Mo_2C@C/CdS, (b) ZnS, and (b') MoS_2-Mo_2C@C/ZnS.